IEEE Access
Multidisciplinary ⋮ Rapid Review ⋮ Open Access Journal

Received 1 June 2023, accepted 15 June 2023, date of publication 19 June 2023, date of current version 27 June 2023.

Digital Object Identifier 10.1109/ACCESS.2023.3287551

RESEARCH ARTICLE

Arbitrary Termination Complex Impedances Tunable Bandpass Filter Using Single and Dual-Mode Resonators

GIRDHARI CHAUDHARY[1], (Member, IEEE), AND YONGCHAE JEONG[2], (Senior Member, IEEE)

[1]JIANT-IT Human Resource Development Center, Division of Electronics Engineering, Jeonbuk National University, Jeonju-si 54896, South Korea
[2]Division of Electronics Engineering, Jeonbuk National University, Jeonju-si 54896, South Korea

Corresponding author: Yongchae Jeong (ycjeong@jbnu.ac.kr)

This work was supported in part by the National Research Foundation of Korea (NRF) Grant funded by the Korean Government (MSIT) under Grant RS-2023-00209081, and in part by the Basic Science Research Program through NRF Grant funded by the Ministry of Education under Grant 2019R1A6A1A09031717.

ABSTRACT This paper presents a design of microstrip line tunable bandpass filter (BPF) with a transmission zero (TZ) that can accommodate arbitrarily terminated input and output port impedances (Z_s and $Z_L \neq 50\ \Omega$). We extracted a new coupling matrix to design the proposed tunable BPF and presented an intuitive circuit-level implementation using a single dc-bias controlled single and dual-mode resonators. The proposed tunable BPF integrates the function of tunable filter and matching network into a single circuit. To validate the design, three filter prototypes with different input and output port termination impedances (filter A: 50-to-50 Ω, filter B: 20-to-50 Ω, and filter C: (25+j10)-to-50 Ω) are manufactured and their performances were measured. The experimental results are consistent with the simulation showing that the passband frequency of the BPF can be tuned from 1.65 GHz to 2.08 GHz (23.06%) with the insertion loss variation from 3.40 dB to 4.69 dB. The proposed tunable BPFs achieved frequency selectivity characteristics by locating the TZ at a lower stopband. The proposed arbitrary terminated tunable BPF can allow direct connection between power amplifier (PA)/low noise amplifier (LNA) and antenna without extra matching networks, resulting in smaller circuit size and can enhance overall performance of RF front-end.

INDEX TERMS Arbitrary termination impedance, bandpass matching network, microstrip coupled line, frequency selective bandpass filter, tunable bandpass filter, transmission zero, varactor diode.

I. INTRODUCTION

Bandpass filters (BPFs) are necessary at output/input of power amplifier (PA)/low noise amplifier (LNA) in RF front-ends to satisfy spectral mask requirements for transmission or reception as shown in Fig. 1(a). In conventional RF front-end, output matching network (OMN) and input matching network (IMN) must be separately designed for PA/LNA and cascaded with 50-to-50 Ω BPF ($Z_s = Z_L = 50\ \Omega$). The insertion losses (ILs) of matching networks and 50-to-50 Ω BPF can increase overall IL and circuit size of RF front-ends. Therefore, it is attractive to consider RF front-end design that integrates BPF and matching network into single circuit so that BPF matching network is directly connected to transistor in RF front-ends, eliminating extra OMN/IMN as shown in Fig. 1(b). The co-design of integrated BPF matching network and PA/LNA can reduce overall circuit size and improve performance of RF front-end. This co-design is only possible if BPFs can be designed considering arbitrary termination (Z_s and $Z_L \neq 50\ \Omega$) impedances. Future RF front-ends are required to support multi-band/standards operations, where integration of tunable BPF and matching network into

The associate editor coordinating the review of this manuscript and approving it for publication was Giorgio Montisci.

a single circuit are key enabling technologies for reducing overall circuit size and improving performances of such systems.

The concept of integrating BPF and matching network into single circuit has been demonstrated using evanescent-mode (EVA) cavity [1], [2], waveguide [3], and substrate-integrated waveguide (SIW) resonators [4]. Additional research in [5] presents second and fourth-order microstrip line BPF integrated matching network around 2.4 GHz. Similarly, coupling matrix synthesis of BPF with arbitrary termination impedances has been presented in [6] and [7] using waveguide resonators. Microstrip line BPF with arbitrary complex termination impedances has been designed and validated in [8] using stepped impedance resonator (SIR) around 2.6 GHz. However, these design concepts of BPF with arbitrary termination impedances have only been demonstrated for fixed passband frequency. It will be more attractive to consider co-design of integrated tunable BPF and matching networks into the single circuit to support multi-band/standard operations of RF front-end.

Several tunable BPF designs have been reported in previous works assuming 50 Ω termination impedances ($Z_s = Z_L = 50\ \Omega$) conditions. For instance, tunable BPFs that used two varactor-tuned switchable resonators were presented in [9] and [10]. A second-order tunable combline BPF with a constant bandwidth was presented in [11] using a T-type bandwidth control network. Similarly, the viability of fourth-order BPFs with constant fractional bandwidth was demonstrated by implementing different coupling mechanisms including cross-coupling between quarter-wavelength and half-wavelength resonators [12], dual zero-value coupling with two coupling paths [13], and changing magnetic coupling to electrical coupling (or vice-versa) in combine resonators [14]. In [15], a microstrip tunable filter with passband frequency and bandwidth controllable was demonstrated using short-circuited coupled lines. Likewise, a design methodology for a frequency-selective tunable BPF that used a dual-mode resonator, and an element variable coupling matrix was presented in [16]. However, these design approaches are not applicable if termination impedances of tunable BPFs are different from 50 Ω.

In recent years, there have been efforts to design higher-order tunable BPF with single dc-bias voltage-controlled tunable resonators. For example, one study demonstrated fourth-order and six-order tunable BPFs with a constant bandwidth [17]. Another study presented a third-order microstrip line tunable BPF that used a single dc-bias control circuit to tune the passband [18]. In [19], a bandwidth switchable BPF that utilized semiconductor-distributed doped areas as an active tunable element was demonstrated. Additionally, a fourth-order tunable BPF with a constant bandwidth was reported in [20], which used an element variable coupling matrix extracted from classical filter polynomials.

Despite the extensive research, previously reported tunable BPFs are designed assuming 50-to-50 Ω ($Z_S = Z_L = 50\ \Omega$) termination impedances, as results, these conventional tunable BPFs cannot integrate the function of tunable BPF and matching network into single circuit.

In this paper, we present a design and experimental validation of arbitrarily terminated input and outport termination impedances microstrip line tunable BPF with transmission zero (TZ) which can integrate functions of tunable BPFs and matching network into a single circuit. To design the proposed arbitrarily terminated tunable BPF, a new coupling matrix (CM) is extracted by modifying the existing CM, and an intuitive circuit level implementation of the proposed tunable BPF is presented using single dc-bias voltage controlled tunable resonators. To enhance frequency selective characteristics, TZ can be located at a lower or higher stopband by using either capacitive or inductive cross-coupling between the resonators. To validate the proposed approach, we designed and manufactured three filter prototypes (filter A: 50-to-50 Ω, filter B: 20-to-50 Ω and filter C: (25+j10)-to-50 Ω) with TZ located at the lower stopband were designed and measured.

II. DESIGN THEORY

Fig. 2 illustrates the coupling diagram of the proposed 3rd-order tunable BPF. The TZs are generated by cross-coupling between the first and last resonators. The (N+2) ×(N+2) CM of the 3rd-order filter with the input and output port impedances are normalized to 1 Ω [21], [22], is given by (1), where self-coupling of the resonators is represented by M_{ii}(i = 1, 2, 3).

$$[M_0] = \begin{bmatrix} 0 & M_{S1} & 0 & 0 & 0 \\ M_{S1} & M_{11} & M_{12} & M_{13} & 0 \\ 0 & M_{12} & M_{22} & M_{23} & 0 \\ 0 & M_{13} & M_{23} & M_{33} & M_{3L} \\ 0 & 0 & 0 & M_{3L} & 0 \end{bmatrix} \tag{1}$$

Using (1), the normalized input/output impedance looking at the input (source) and output (load) port is expressed as (2).

$$z_{in} = \frac{M_{3L}^2\left(M_{12}^2 - M_{13}M_{22}\right)^2 + jM_{11}}{M_{S1}^2\left(M_{12}^2 - M_{33}M_{22}\right)^2 + M_{S1}^2M_{22}^2M_{3L}^4} \tag{2a}$$

$$z_{out} = \frac{M_{S1}^2\left(M_{12}^2 - M_{13}M_{22}\right)^2 + jM_{33}}{M_{3L}^2\left(M_{12}^2 - M_{33}M_{22}\right)^2 + M_{3L}^2M_{22}^2M_{S1}^4} \tag{2b}$$

Assuming $M_{22} = M_{33} = 0$, the input impedance looking at the input (source) port is further simplified as (3).

$$z_{in} = \frac{M_{3L}^2 + jM_{11}}{M_{S1}^2} \tag{3}$$

By examining (3), it is apparent that it is possible to design a filter with an arbitrary termination impedance by modifying M_{S1} and M_{11}, while preserving the same Chebyshev response with TZ. Hence, the CM of frequency tunable BPF with arbitrary source and load normalized

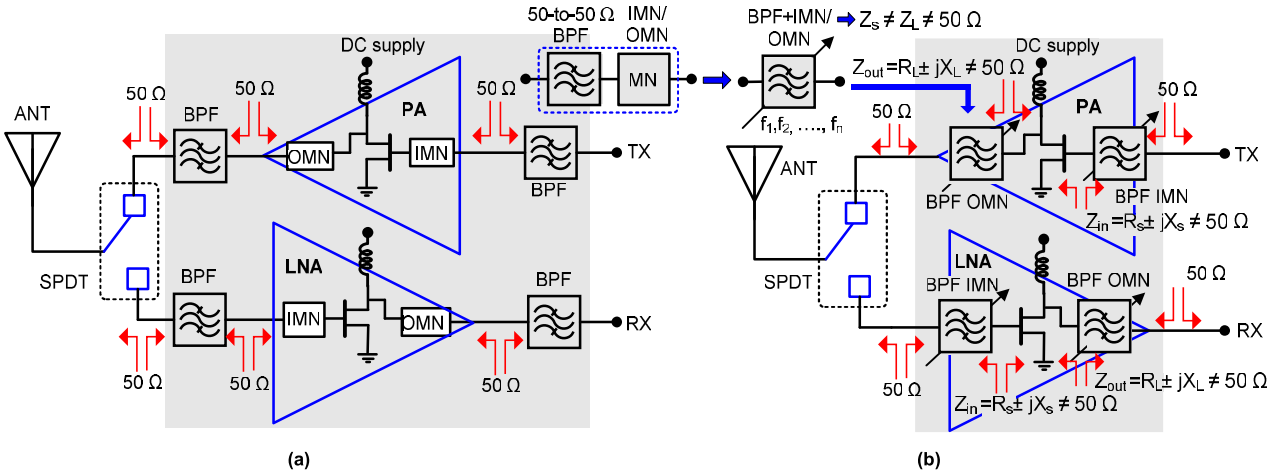

FIGURE 1. Block diagrams: (a) conventional RF front end where PA/LNA with output matching network (OMN)/input matching network (IMN) are cascaded with $Z_S = Z_L = 50\ \Omega$ BPF and (b) block diagram of the proposed tunable RF front-end where arbitrary terminated tunable BPFs (Z_S and $Z_L \neq 50\ \Omega$) are directly connected transistor as BPF OMN and BPF IMN, resulting elimination of extra OMN and IMN of PA/LNA and reducing overall circuit size.

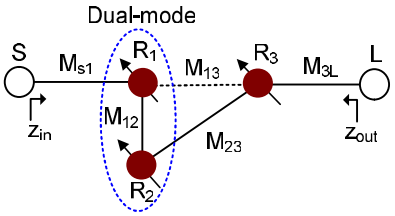

FIGURE 2. Coupling diagram of the proposed tunable BPF using dual-mode and single-mode resonators.

impedances is represented by (4).

$$[M_{new}] = \begin{bmatrix} 0 & M'_{S1} & 0 & 0 & 0 \\ M'_{S1} & M'_{11}+x & M_{12} & M_{13} & 0 \\ 0 & M_{12} & M_{22}+x & M_{23} & 0 \\ 0 & M_{13} & M_{23} & M'_{33}+x & M'_{3L} \\ 0 & 0 & 0 & M'_{3L} & 0 \end{bmatrix} \tag{4}$$

where x is the tuning element of the self-resonant frequency of resonator. Using (4), the input impedance looking at the source port is obtained as (5).

$$z_{in} = r_s + jx_s = \frac{M_{3L}^2 + jM'_{11}}{M'^2_{S1}}, \tag{5}$$

The normalized real and imaginary part of source termination impedance are represented by r_s and x_s, respectively. If the values of M_{S1} and M_{11} are adjusted, the frequency response of filter with arbitrarily connected input port impedance $(r_s + jx_s)$, will be unchanged. To this end, the modified values of M_{S1} and M_{11} can be derived using (3) and (5) as given in (6).

$$M'_{S1} = \frac{M_{S1}}{\sqrt{r_s}}, \quad M'_{11} = M_{11} - \frac{x_s}{r_s} M_{S1}^2 \tag{6}$$

In a similar manner, it is possible to obtain frequency response when output port is connected to an arbitrary normalized termination impedances $(r_L + jx_L)$ by adjusting the values of M_{3L} and M_{33}. Thus, the modified values M_{3L} and M_{33} can be derived as shown in (7).

$$M'_{3L} = \frac{M_{3L}}{\sqrt{r_L}}, \quad M'_{33} = M_{33} - \frac{x_L}{r_L} M_{3L}^2 \tag{7}$$

Equations (6) and (7) reveal that the arbitrarily terminated complex port impedances are matched by detuning the resonant frequency of first and last resonators, as given in (8).

$$f_{0i} = f_c \left\{ \sqrt{1 + \left(\frac{\Delta M'_{ii}}{2} \right)^2} + \frac{\Delta M'_{ii}}{2} \right\}, \quad i = 1, 3 \tag{8}$$

Similarly, the location of TZ frequency can be determined using (9).

$$f_{TZ} = f_c \left\{ \sqrt{1 + \frac{\Delta^2}{f_c^2} \left(\frac{M_{12}M_{23} - M_{13}M_{22}}{2M_{13}} \right)^2} + \frac{\Delta}{f_c} \cdot \frac{M_{12}M_{23} - M_{13}M_{22}}{2M_{13}} \right\} \tag{9}$$

Equation (9) shows that location of the TZ can be adjusted by controlling M_{13}, which represents cross-coupling between resonator R_1 and R_3. The position of the TZ at a lower or higher stopband is determined by the polarity of M_{13}, which can be negative or positive. Therefore, the TZ can be located at a lower stopband with negative value of M_{13} or at a higher stopband with positive value of M_{13}.

A. DESIGN EXAMPLE 1: TZ AT LOWER STOPBAND FREQUENCY

Several tunable BPFs with TZ located at lower stopband frequency have been designed and simulated using a CM.

The target specifications for these tunable BPF are given as follows:

1) *Transfer function: 3rd-order chebyshev with passband return loss (RL) of 20 dB*
2) *Equiripple bandwidth (BW): 110 MHz*
3) *Transmission zero (TZ) at located lower stopband with normalized frequency $\Omega_{TZ} = -6.02$ rad/s.*
4) *Input and output port termination impedances: filter A: 50-to-50 Ω ($Z_S = Z_L = 50$ Ω), filter B: 75-to-50 Ω ($Z_S = 75$ Ω and $Z_L = 50$ Ω), filter C: (25+j10)-to-50 Ω ($Z_S = 25+j10$ Ω and $Z_L = 50$ Ω) and filter D: (25+j10)-to-(55-j20) Ω ($Z_S = 25+j10$ Ω and $Z_L = 55-j20$ Ω).*
5) *Passband frequency tuning range: 1.60 GHz to 2.05 GHz*

The CM $[M_0]$ with a reference impedance of 1 Ω synthesized using filter synthesis theory [21] based on these specifications. The resulting CM can be expressed as (10).

$$\begin{bmatrix} 0 & 1.0825 & 0 & 0 & 0 \\ 1.0825 & -0.045+x & 1.0189 & -0.1775 & 0 \\ 0 & 1.0189 & 0.1736+x & 1.0189 & 0 \\ 0 & -0.1775 & 1.0189 & -0.045+x & 1.0825 \\ 0 & 0 & 0 & 1.0825 & 0 \end{bmatrix} \tag{10}$$

The CM of filter A (50-to-50 Ω) remained the same as (10). However, the CM of filter B (75-to-50 Ω), filter C (25+j10-to-50 Ω), and filter D ((25+j10)-to-55−j20 Ω) are calculated as (11a),(11b) and (11c), respectively, using (6), (7), and (10).

$$\begin{bmatrix} 0 & 0.8838 & 0 & 0 & 0 \\ 0.8838 & -0.045+x & 1.0189 & -0.1775 & 0 \\ 0 & 1.0189 & 0.1736+x & 1.0189 & 0 \\ 0 & -0.1775 & 1.0189 & -0.045+x & 1.0825 \\ 0 & 0 & 0 & 1.0825 & 0 \end{bmatrix} \tag{11a}$$

$$\begin{bmatrix} 0 & 1.5309 & 0 & 0 & 0 \\ 1.5309 & -0.5137+x & 1.0189 & -0.1775 & 0 \\ 0 & 1.0189 & 0.1736+x & 1.0189 & 0 \\ 0 & -0.1775 & 1.0189 & -0.045+x & 1.0825 \\ 0 & 0 & 0 & 1.0825 & 0 \end{bmatrix} \tag{11b}$$

$$\begin{bmatrix} 0 & 1.5309 & 0 & 0 & 0 \\ 1.5309 & -0.5137+x & 1.0189 & -0.1775 & 0 \\ 0 & 1.0189 & 0.1736+x & 1.0189 & 0 \\ 0 & -0.1775 & 1.0189 & 0.3811+x & 1.0321 \\ 0 & 0 & 0 & 1.0321 & 0 \end{bmatrix} \tag{11c}$$

The S-parameter results of filter A, B, C, and D are shown in Fig. 3, where TZ is located at a lower stopband. The passband frequency can be tuned from 1.61 GHz to 2.05 GHz. Furthermore, the S-parameter results show that the filter response remains almost identical even though the input and output port impedances are chosen arbitrary. These findings suggest that by modifying the external Q-factors and detuning the resonant frequencies of the first/last resonators, a 3rd-order BPF with arbitrary input and output port impedances can be designed.

B. DESIGN EXAMPLE 2: TZ AT HIGHER STOPBAND FREQUENCY

Design example 2 involves designing and simulating several 3rd-order tunable BPFs with TZ at higher stopband frequency. The target specifications are the same as in design example 1 except for the location of TZ. The CM of the designed BPF with TZ located at a normalized frequency of $\Omega_{TZ} = 6.02$ rad/s is calculated using (12).

$$\begin{bmatrix} 0 & 1.0825 & 0 & 0 & 0 \\ 1.0825 & 0.0452+x & 1.0188 & 0.1782 & 0 \\ 0 & 1.0188 & -0.1743+x & 1.0188 & 0 \\ 0 & 0.1782 & 1.0188 & 0.0452+x & 1.0825 \\ 0 & 0 & 0 & 1.0825 & 0 \end{bmatrix} \tag{12}$$

Consistent with design example 1, the CM of filter A (50-to-50 Ω) remained the same as that in (12), however, the coupling matrices of filter B (75-to-50 Ω), filter C (25+j10-to-50 Ω), and filter D ((25+j10)-to-55-j20 Ω) are calculated as (13) using (6), (7), and (12).

$$\begin{bmatrix} 0 & 0.8838 & 0 & 0 & 0 \\ 0.8838 & 0.0452+x & 1.0188 & 0.1782 & 0 \\ 0 & 1.0188 & -0.1743+x & 1.0188 & 0 \\ 0 & 0.1782 & 1.0188 & 0.0452+x & 1.0825 \\ 0 & 0 & 0 & 1.0825 & 0 \end{bmatrix} \tag{13a}$$

$$\begin{bmatrix} 0 & 1.5309 & 0 & 0 & 0 \\ 1.5309 & -0.4335+x & 1.0188 & 0.1782 & 0 \\ 0 & 1.0188 & -0.1743+x & 1.0188 & 0 \\ 0 & 0.1782 & 1.0188 & 0.0452+x & 1.0825 \\ 0 & 0 & 0 & 1.0825 & 0 \end{bmatrix} \tag{13b}$$

$$\begin{bmatrix} 0 & 1.5309 & 0 & 0 & 0 \\ 1.5309 & -0.4335+x & 1.0188 & 0.1782 & 0 \\ 0 & 1.0188 & -0.1743+x & 1.0188 & 0 \\ 0 & 0.1782 & 1.0188 & 0.4713+x & 1.0321 \\ 0 & 0 & 0 & 1.0321 & 0 \end{bmatrix} \tag{13c}$$

The synthesized CM S-parameter results of filter A, filter B, filter C, and filter D are shown in Fig. 3. In these simulation results, TZ is located at a higher stopband. The passband frequency was tuned from 1.61 GHz to 2.05 GHz. Similar to the previous case, the S-parameter results remained almost unchanged despite the arbitrary source and load termination impedances.

C. DESIGN EXAMPLE 3: TZ CLOSE TO PASSBAND AT LOWER STOPBAND FREQUENCY

The target specifications are identical to those in design example 1 except for the location of TZ. The CM of the

3rd-order BPF with TZ located at a normalized frequency of $\Omega_{TZ} = -3$ rad/s (close to passband) is calculated as (14).

$$\begin{bmatrix} 0 & 1.0826 & 0 & 0 & 0 \\ 1.0826 & -0.0908+x & 0.9818 & -0.3642 & 0 \\ 0 & 0.9818 & 0.3532+x & 0.9818 & 0 \\ 0 & -0.3642 & 0.9818 & -0.0908+x & 1.0826 \\ 0 & 0 & 0 & 1.0826 & 0 \end{bmatrix} \tag{14}$$

Consistent with design example 1, the CM of filter A (50-to-50 Ω) remained the same as that in (14). However, the CM of filter B (75-to-50 Ω) and filter C ((25+j10)-to-50 Ω) are calculated as (15) using (6), (7), and (14).

$$\begin{bmatrix} 0 & 0.8838 & 0 & 0 & 0 \\ 0.8838 & -0.0908+x & 0.9818 & -0.3642 & 0 \\ 0 & 0.9818 & 0.3532+x & 0.9818 & 0 \\ 0 & -0.3642 & 0.9818 & -0.0908+x & 1.0826 \\ 0 & 0 & 0 & 1.0826 & 0 \end{bmatrix} \tag{15a}$$

$$\begin{bmatrix} 0 & 1.5310 & 0 & 0 & 0 \\ 1.5310 & -0.5596+x & 0.9818 & -0.3642 & 0 \\ 0 & 0.9818 & 0.3532+x & 0.9818 & 0 \\ 0 & -0.3642 & 0.9818 & -0.0908+x & 1.0826 \\ 0 & 0 & 0 & 1.0826 & 0 \end{bmatrix} \tag{15b}$$

Fig. 4 depicts the simulated CM frequency response of filter A, filter B, and filter C when TZ is located close to passband. Despite TZ being located close to passband, the passband frequency can still be tuned from 1.61 GHz to 2.05 GHz, which is same design example 1. Consistent with the previous case, the S-parameter results remained nearly identical even though the input and output port impedances are arbitrary and TZ is close to passband.

D. DESIGN EXAMPLE 4: FILTERS WITH FREQUENCY-DEPENDENT PORT IMPEDANCES

To investigate the effect of frequency-dependent input/output port impedances in passband frequency tunable range, three filters (filter A: 50-to-50 Ω, filter B: 75-to-50 Ω, and filter C: (25+j10)-to-50 Ω) are designed and simulated. The target specifications are identical to those in design example 3, so the CM of these three BPFs are same as in (14) and (15). Using these frequency-dependent port impedances ($R_S \mp j\omega X_S$) where $R_S = 50/75/25$ Ω and $X_S = -5$ to 5 Ω, Fig. 5 shows the simulated CM frequency response of tunable BPFs. Fig. 6 shows smith-chart results of frequency-independent and frequency-dependent port impedances. It should be noted that the return loss is slightly degraded at lower and upper passband frequencies, but the passband frequency tunability remains identical to that with frequency-independent port impedances.

III. MICROSTRIP LINE TUNABLE FILTER IMPLEMENTATION

Following sections will describe the microstrip line implementation of the proposed tunable BPF.

A. RESONANT FREQUENCY ANALYSIS OF SINGLE AND DUAL-MODE TUNABLE RESONATORS

The proposed structure of dual-mode tunable resonator is shown in Fig. 7(a). It consists of three series transmission lines (TLs) with characteristic impedances and electrical lengths of Z_1, Z_2, θ_0, θ_1, θ_2, along with a varactor diode having a capacitance of C_v at a specific dc bias voltage and a short-circuited shunt stub TL with characteristic impedance Z_k and electrical length of θ_{k1}. Using even-and odd-mode analysis, Fig. 8 depicts even and odd-mode equivalent circuits of the proposed dual-mode resonator. Using these equivalent circuits, the even-and odd-mode input admittances are derived as (16).

$$Y_{ine} = jY_2 \frac{Y_L^e + Y_2 \tan\theta_2}{Y_2 - Y_L^e \tan\beta\theta_2} \tag{16a}$$

$$Y_{ino} = jY_2 \frac{Y_L^o + Y_2 \tan\theta_2}{Y_2 - Y_L^o \tan\theta_2} \tag{16b}$$

where

$$Y_L^e = Y_1 \frac{Y_{in}^e + Y_1 \tan\theta_1}{Y_1 - Y_{in}^e \tan\theta_1}, \quad Y_L^o = Y_1 \frac{Y_{in}^o + jY_1 \tan\theta_1}{Y_1 - Y_{in}^o \tan\theta_1} \tag{17a}$$

$$Y_{in}^e = \frac{\omega C_v A}{\omega C_v \left(2Y_1 + Y_k \cot\theta_{k1} \tan\theta_0\right) + A} \tag{17b}$$

$$A = 2Y_1^2 \tan\theta_0 - Y_k Y_1 \cot\theta_{k1} \tag{17c}$$

$$Y_{in}^o = \frac{\omega C_v Y_1 \cot\theta_0}{Y_1 \cot\theta_0 - \omega C_v} Y_1 = \frac{1}{Z_1}, \quad Y_2 = \frac{1}{Z_2}. \tag{17d}$$

and ω is the operating frequency of the resonator. The even- and odd-mode resonant frequencies (f_e and f_o) can be solved by setting $im(Y_{ine}) = 0$ and $im(Y_{ino}) = 0$.

Fig. 7(b) shows the proposed structure of a single-mode $\lambda/4$ resonator. The input admittance of single-mode resonator is same as (16b), where the input admittance of single-mode tunable resonator is denoted as $Y_{in} = Y_{ino}$. The resonant frequency of single-mode resonator can be solved by setting $im(Y_{in}) = 0$. Fig. 9 shows calculated resonant frequencies of both dual-mode and single-mode resonators. As observed from these graphs, the resonant frequencies decrease as the capacitance of varactor diode C_v increases.

B. EXTRACTION OF COUPLING COEFFICIENT

Fig. 10(a) depicts the coupling configuration between resonators R_1 and R_2. The resonators are coupled through a short-circuited TL shunt stub with a characteristic impedance of Z_k and an electrical length of θ_{k1}. As the short-circuited shunt TL acts as impedance inverter [23], the coupling strength can be adjusted by varying Z_k and θ_{k1}, keeping Z_1, Z_2, θ_1, θ_2, and θ_0 constant.

Similarly, Fig. 10(b) illustrates the coupling between resonators R_2 and R_3. Resonator R_2 is coupled to resonator

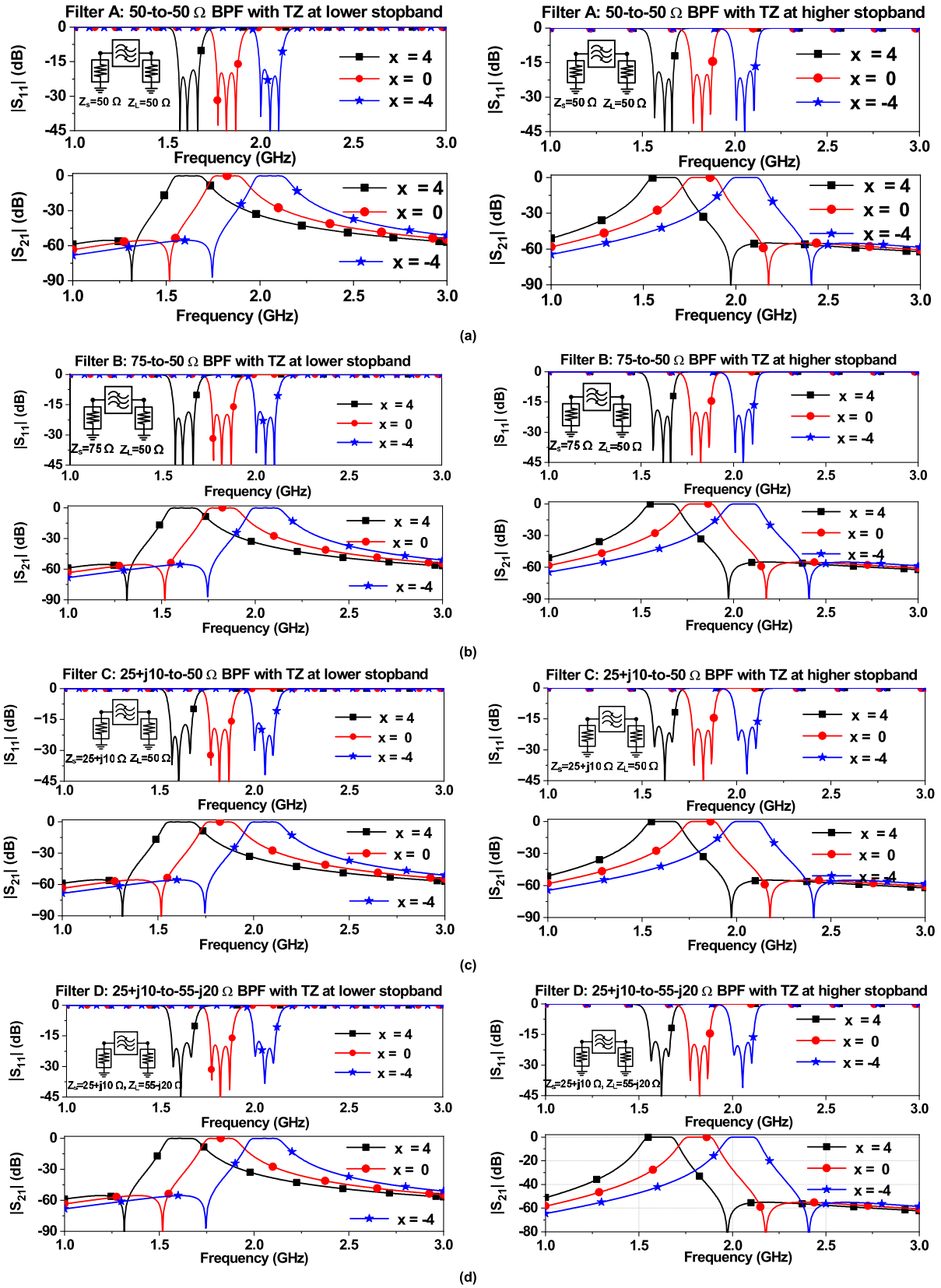

FIGURE 3. Coupling matrix S-parameter results of the proposed tunable BPFs: (a) filter A: 50-to-50 Ω, (b) filter B: 75-to-50 Ω, (c) filter C: (25+j10)-to-50 Ω, and (d) filter D: (25+j10)-to-(55−j20) Ω. The transmission zeros (TZ) are located at lower or higher stopband frequency.

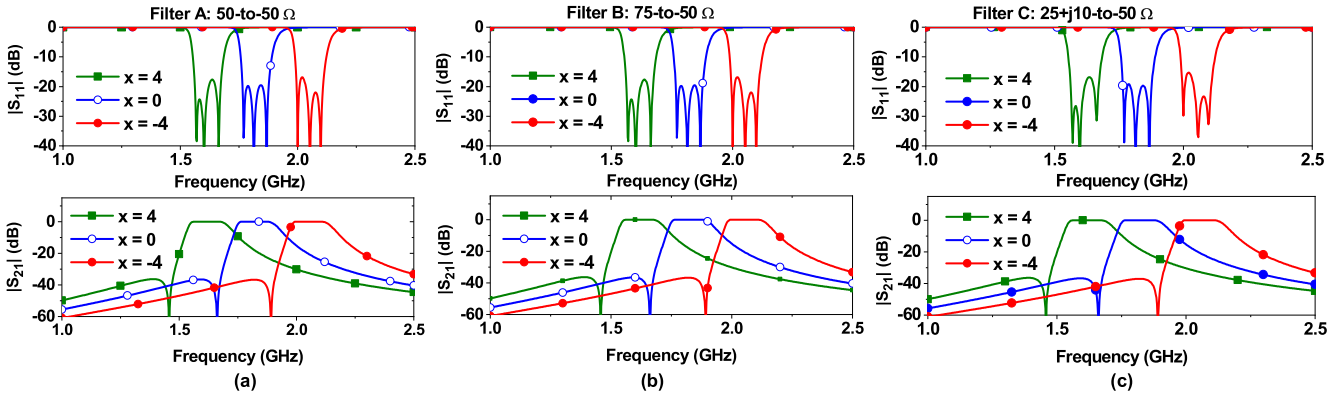

FIGURE 4. Coupling matrix S-parameter results of filters when TZ is located close to passband: (a) filter A: 50-to-50 Ω, (b) filter B: 75-to-50 Ω, and (c) filter C: (25+j10)-to-50 Ω.

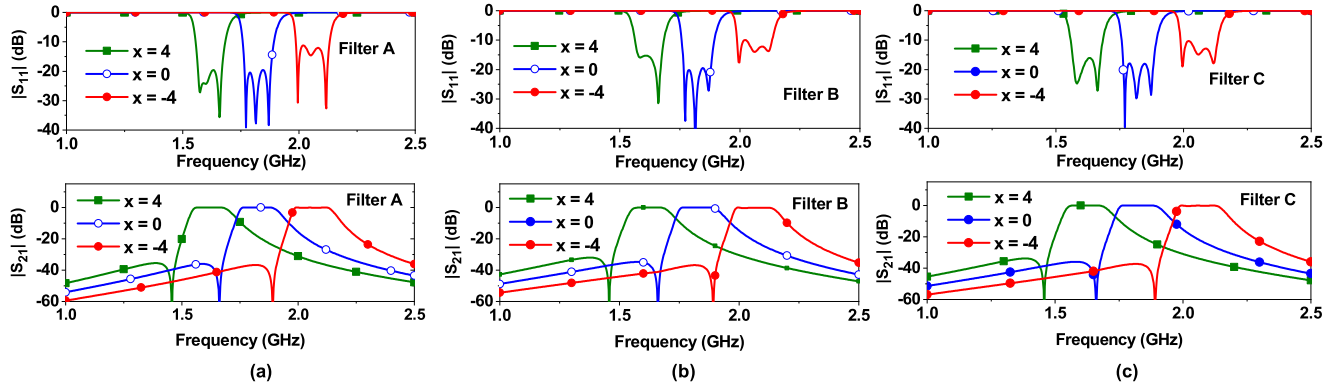

FIGURE 5. Synthesized coupling matrix *S*-parameter results of tunable BPFs with frequency-dependent port impedances ($R_S \mp j\omega X_S$) where $R_S = 50/20/25\ \Omega$ and $X_S = -5$ to 5 Ω (a) filter A, (b) filter B, and (c) filter C.

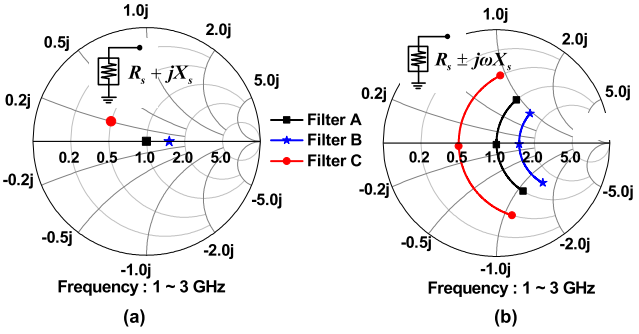

FIGURE 6. (a) Frequency-independent and (b) frequency-dependent port impedance for designed tunable BPFs.

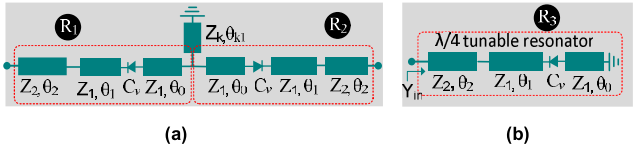

FIGURE 7. Proposed structure of tunable resonators: (a) dual-mode and (b) λ/4 single mode resonator.

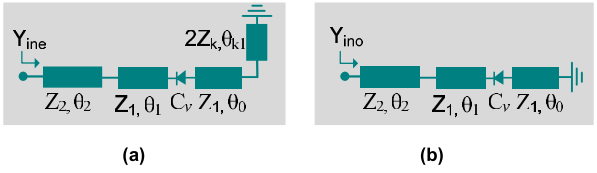

FIGURE 8. Equivalent circuit of dual-mode resonator under: (a) even-mode excitation and (b) odd-mode excitation.

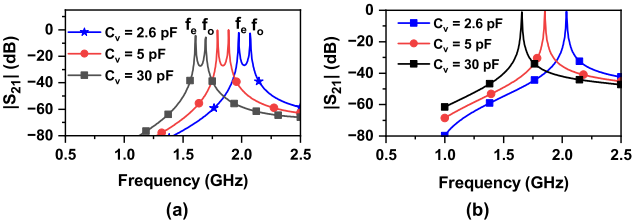

FIGURE 9. (a) Resonant frequencies of dual-mode resonator and (b) resonant frequencies of single-mode resonator. Circuit parameters: $Z_1 = Z_2 = Z_k = 70\ \Omega$, $\theta_0 = 15°$, $\theta_1 = 40°$, $\theta_2 = 25°$, $\theta_{k1} = 2.2°$.

R_3 through the coupled line with even- and odd-mode impedances of $Z_{0e2} = 1/Y_{0e2}$ and $Z_{0o2} = 1/Y_{0o2}$ and an electrical length of θ_2. The coupled line is equivalent to frequency-dependent admittance inverter, and the coupling strength between resonators R_2 and R_3 can be adjusted by changing the values of Z_{0e2} and Z_{0o2}, while keeping the other parameters constant. The coupling coefficient $|m_{ij}|$ can be

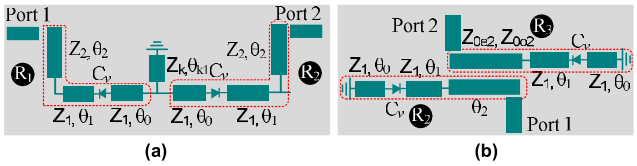

FIGURE 10. Coupling configurations: (a) coupling between resonators R_1 and R_2, and (b) coupling between resonators R_2 and R_3.

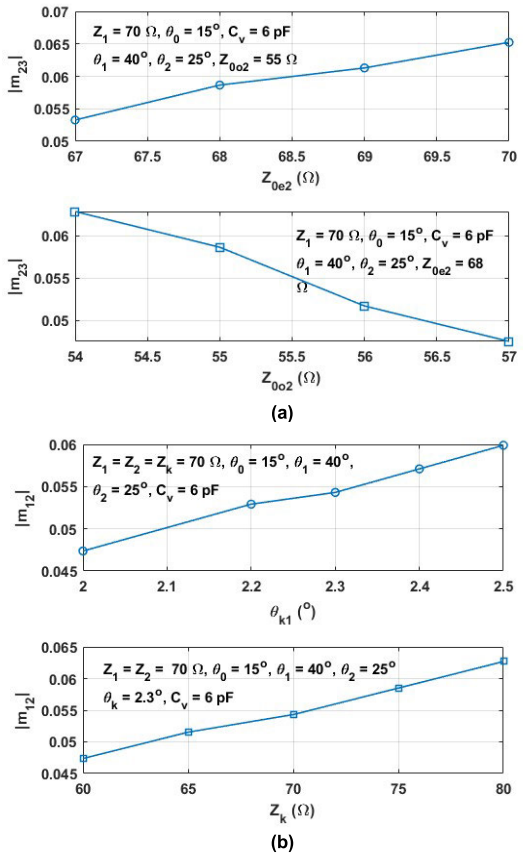

FIGURE 11. Extracted coupling coefficient: (a) coupling coefficient between resonators R_1 and R_2, and (b) coupling coefficient between resonators R_2 and R_3.

determined using (18).

$$|m_{ij}| = \frac{f_h^2 - f_l^2}{f_h^2 + f_l^2}, \quad \text{for } i, j = 1, 2 \tag{18}$$

where f_h and f_l are higher and lower frequency peaks respectively, appearing in $|S_{21}|$ of two synchronously coupled resonators [21]. Fig. 11(a) shows the variation of extracted coupling coefficient ($|m_{12}|$) between resonators R_1 and R_2 as function of Z_k and θ_{k1}, while Fig. 11(b) illustrates the extracted coupling coefficient ($|m_{23}|$) between resonators R_2 and R_3 with respect to Z_{0e2} and Z_{0o2}. The circuit parameters used in extraction are provided in the figure.

The coupling coefficient between R_1 and R_2 increases with increasing in Z_k and θ_{k1}. On the hand the coupling coefficient between R_2 and R_3 decreases with increase in Z_{0e2}, but decreases with increasing values of Z_{0o2}

C. EXTRACTION OF INPUT/OUTPUT EXTERNAL QUALITY (Q) FACTORS

Fig. 12(a) illustrates the circuit implementation of the coupling between input port and resonator R_1 achieved through a series TL (Z_S, θ_S) and a coupled line (Z_{0e1}, Z_{0o1}) with an electrical length of θ_2. Fig. 12(b) shows the circuit implementation of the coupling between the output port and resonator R_3, accomplished through a series TL (Z_L, θ_L) and taping position θ_{k2} of a short-circuited TL with characteristic impedance Z_k. The external quality Q-factors at input and outputs can be determined through well-known expression [22].

$$Q_{eS/eL} = \frac{\omega_0 \tau_{s11}(\omega_0)}{4} \tag{19}$$

where $\tau_{s11}(\omega_0)$ is group delay of S_{11} at resonant angular frequency ω_0.

As the figure suggests, the required input external quality (Q) factor can be determined by selecting appropriate value of Z_S, θ_s Z_{0e1}, and Z_{0o1}. Similarly, the required output external Q-factor can be obtained by controlling Z_L, θ_L, Z_k, and θ_{k2}.

Fig. 13(a) shows the extracted input external Q-factor as in relation to Z_S, θ_S Z_{0e1}, and Z_{0o1}. The input external Q-factor (Q_{eS}) decreases as Z_{0e1} and θ_s increases, but increases as Z_{0o1} rises. On other hand, Fig. 13(b) depicts impact of Z_k, Z_L and θ_{k2} on output external Q-factor (Q_{eL}). As Z_k and θ_{k2} increase, the output external Q-factor decreases. Conversely, as Z_L increases, the output external Q-factor also decreases. When cross-coupling capacitor C_c is considered, the external Q-factors are slightly increased, depending on location of TZ.

D. DESIGN PROCEDURES OF ARBITRARY TERMINATED TUNABLE BPF

The design procedure of the proposed tunable BPF with TZ and arbitrary termination impedances can be summarized as follows:

a) Begin by selecting the desired filter specifications, including source/load termination impedance, return loss (RL), bandwidth (Δ), and TZ position. Then, extract the CM and coupling coefficient based on filter specifications.
b) Choose appropriate circuit parameters for the resonator using (16) to achieve the desired passband frequency tunability of the resonator.
c) Determine the required coupling coefficients (m_{12} and m_{23}) based on (18) with the design figures (e.g. Fig. 11).
d) Extract the required external Q-factors (Q_{eS} and Q_{eL}) using (19) and design figures (e.g. Fig. 13).
e) Finally, optimize the physical dimensions using EM simulator to meet the prescribed RL level and TZ positions.

To demonstrate the feasibility of the proposed tunable BPF with arbitrary input and output port impedances, we designed

TABLE 1. Circuit parameters of the proposed tunable BPF with TZ and arbitrary termination impedances.

Filter A: 50-to-50 Ω		Filter B: 75-to-50 Ω		Filter C: (25+j10)-to-50 Ω	
$Z_1 = Z_k = Z_S = Z_L = 70\ \Omega$, $\theta_0 = 12.66°$, $\theta_1 = 40°$, $\theta_2 = 25°$, $\theta_L = 50°$, $\theta_{01} = 1.95°$, $C_v = 2.6 \sim 30$ pF, Z_{0e2}/Z_{0o2} =67.89/54.57 Ω					
$\theta_S = 38.1°$, $\theta_{k1} = 2.28°$ $\theta_{k2} = 13.24°$ $Z_{0e1}/Z_{0o1} = 100.78/43.74\ \Omega$		$\theta_S = 41.3°$, $\theta_{k1} = 2.54°$, $\theta_{k2} = 13.92°$, $Z_{0e1}/Z_{0o1} = 114.54/40.96\ \Omega$		$\theta_S = 40.6°$, $\theta_{k1} = 2.52°$, $\theta_{k2} = 13.75°$ $Z_{0e1}/Z_{0o1} = 81.2/45.9\ \Omega$	
Transmission zero locations					
at lower stopband	at higher stopband	at lower stopband	at higher stopband	at lower stopband	at higher stopband
$C_c = 6$ fF	$L_L = 20$ nH	$C_c = 4.5$ fF	$L_L = 20.5$ nH	$C_c = 5$ fF	$L_L = 41.5$ nH
Electrical lengths of TLs are defined at 1.50 GHz					

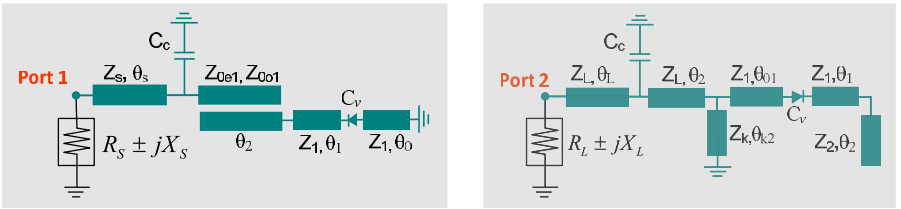

FIGURE 12. Coupling between input/output port and resonator: (a) input external Q-factor and (b) output external Q-factor.

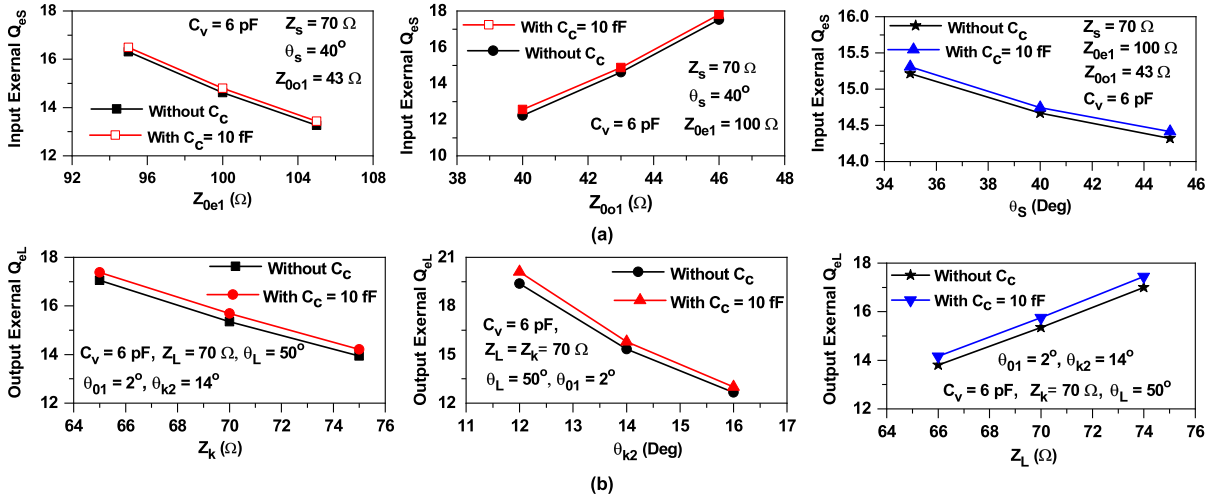

FIGURE 13. Extracted input and output external quality factors with $Z_1 = Z_2 = 70\ \Omega$, $\theta_1 = 40°$, $\theta_2 = 25°$, $\theta_0 = 15°$, $C_V = 6$ pF: (a) input external Q-factor and (b) output external Q-factor.

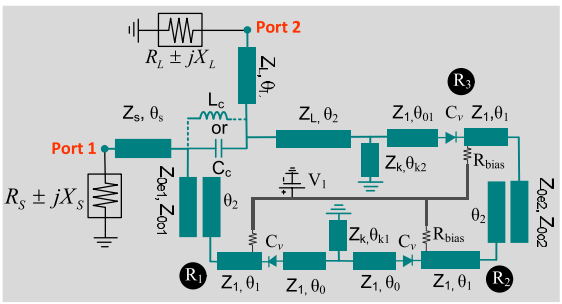

FIGURE 14. Microstrip line implementation of the proposed 3-pole frequency tunable BPF with TZ and arbitrary termination port impedances.

three BPFs (filter A: 50-to-50 Ω, filter B: 75-to-50 Ω, and filter C: (25+j10)-to-50 Ω) with TZ. The filter specifications provided in sections II. The CM for these filters is given in (12)-(15).

Fig. 14 depicts the microstrip implementation of the proposed tunable BPF. The resonator R_1 and R_2 are realized using dual-mode resonator, while R_3 employs a $\lambda/4$ tunable resonator. The circuit parameters of the designed BPFs are provided in Table 1. The cross-coupling between resonators R_1 and R_3 is accomplished using a capacitor or an inductor, depending on the desired location of TZ. Negative coupling between resonators R_1 and R_3 generates TZ at a lower stopband, whereas positive coupling between R_1 and R_3 generates TZ at a higher stopband. Therefore, the implementing coupling between R_1 and R_3 with a capacitor (C_c) generates TZ at a lower stopband, while using an inductor (L_c) between resonator R_1 and R_3 generates TZ at a higher stopband.

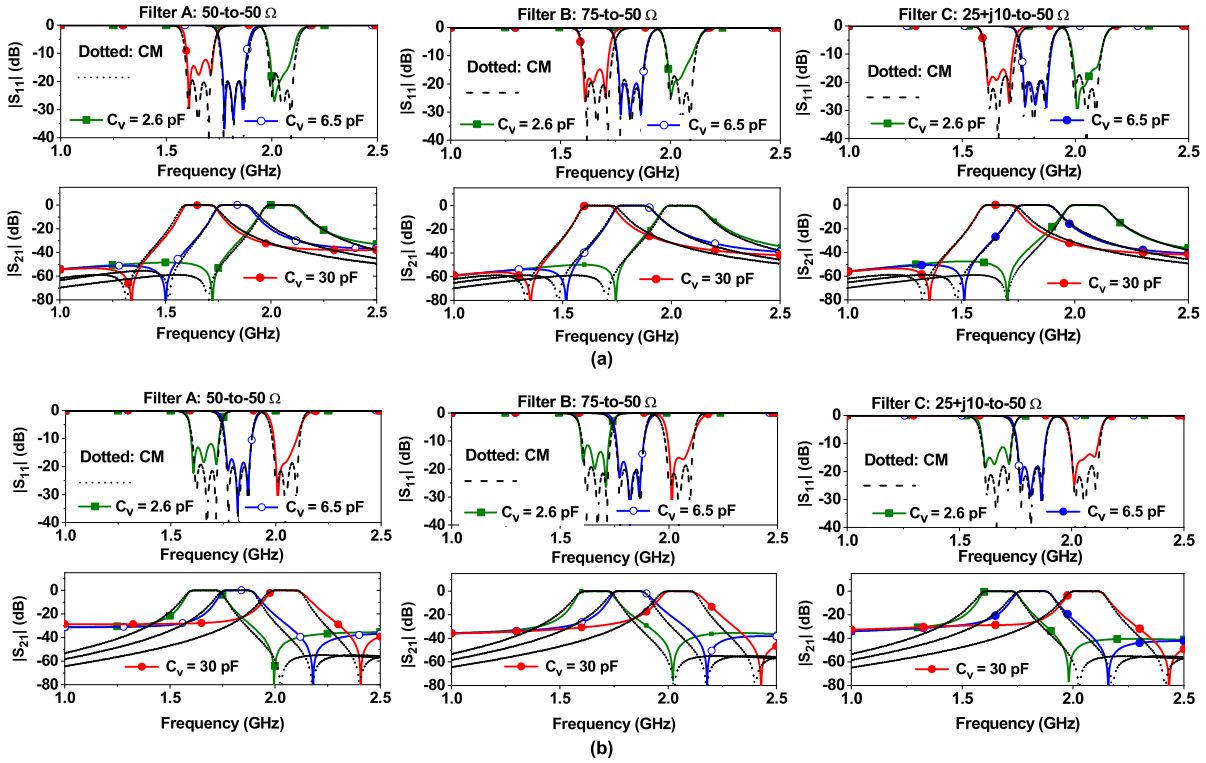

FIGURE 15. Comparison between synthesized CM and microstrip line tunable BPFs simulation results: (a) TZ at lower stopband and (b) TZ at higher stopband.

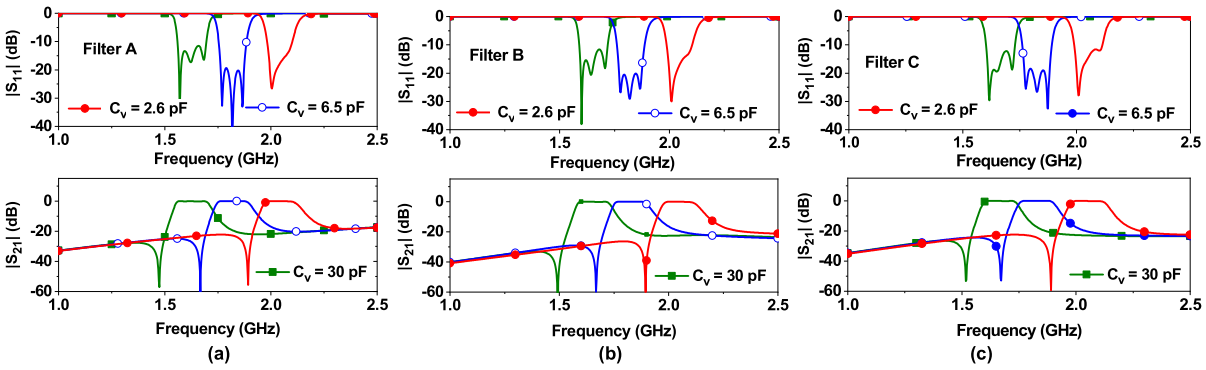

FIGURE 16. Simulation results of microstrip line tunable BPF with frequency-dependent port impedances ($R_S \mp j\omega X_S$) where R_S = 50/75/25 Ω and $X_S = -5$ to 5 Ω (a) filter A, (b) filter B, and (c) filter C.

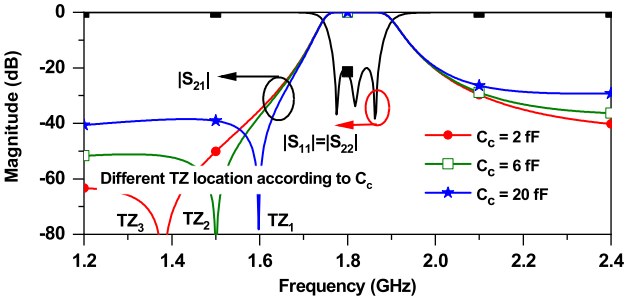

FIGURE 17. Different transmission zeros (TZs) locations microstrip line tunable BPF according to C_c.

To compare the synthesized CM and physically implemented microstrip line BPF frequency responses, the simulation results of BPF with TZ located at different stopband frequencies are shown in Fig. 15. Fig. 15(a) displays the simulation results of BPF with TZ located at a lower stopband, while Fig. 15(b) shows the simulation results with TZ located at a higher stopband. The synthesized CM results are very consistent with frequency response of the physically implemented BPFs.

To investigate effect of frequency-dependent port impedances on passband frequency tunability, three microstrip line BPF with different input and output port impedance (filter A: 50-to-50 Ω, filter B: 75-to-50 Ω, and filter C: (25+j10)-to-50 Ω) are designed and simulated. The frequency dependent-port impedance of the tunable BPF is chosen as $Z_s = (R_S \mp j\omega X_S)$, where $R_S = 50/75/25\Omega$, and $X_S = -5$ to 5 Ω. Fig. 16 shows the simulation results of these

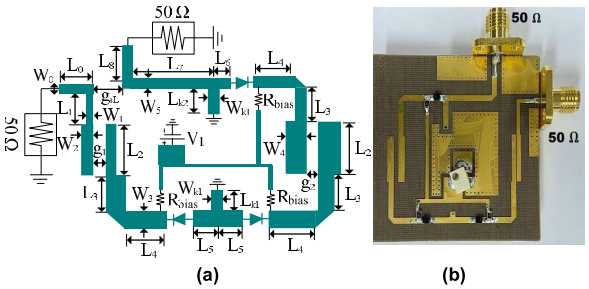

FIGURE 18. (a) Physical layout and (b) photograph of fabricated filter A. Physical dimenstions: $W_0 = W_1 = 0.9$, $W_2 = 1.14$, $W_3 = 1.36$, $W_{k1} = 1.4$, $W_4 = 1.71$, $W_5 = 1.36$, $L_0 = 6$, $L_1 = 7.1$, $L_2 = 10.76$, $L_3 = 8$, $L_4 = 8$, $L_5 = 5.97$, $L_{k1} = 1.3$, $L_{k2} = 6.40$, $L_6 = 1.05$, $L_7 = 11.3$, $L_8 = 9$, $g_1 = 0.13$, $g_2 = 1.08$, $g_{sL} = 3.13$. Unit: millimeter (mm).

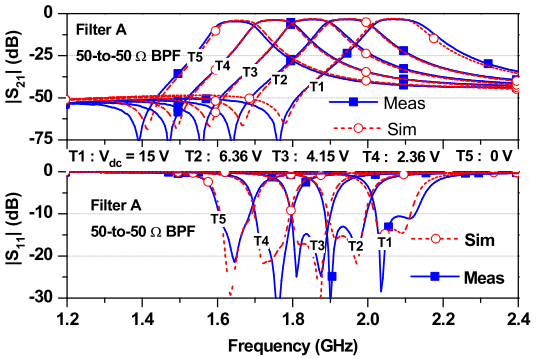

FIGURE 19. Simulation and measurement results of filter A: 50-to-50 Ω.

BPFs. As observed from these results, the passband frequency is tuned from 1.65 GHz to 2.05 GHz with slight- degradation in return loss at lower and upper passband frequencies due to the frequency-dependent port impedances.

Fig. 17 shows simulation results of the proposed BPF with different C_c. In this simulation, the passband center frequency is kept constant at 1.82 GHz. As value of C_c decreases, the negative coupling between resonators R_1 and R_3 decreases, resulting in the TZ location shifted away from passband.

IV. EXPERIMENTAL RESULTS

For experimental verification, three prototypes of tunable BPFs with TZ located in the lower stopband (filter A: 50-to-50 Ω, filter B: 20-to-50 Ω, and filter C: 25+j10-to-50 Ω) are designed fabricated on a Taconic substrate with $\varepsilon_r = 2.2$, $h = 31$ mils, and loss tangent $(\tan\delta) = 0.0009$. The variable capacitor was implemented using varactor diode SMV-1233 from Skyworks Inc, which provided the capacitance variation of 1 pF to 20 pF with a reverse bias voltage of 15 V to 0 V. The electromagnetic simulator ANSYS HFSS 2020 and the Keysight Advanced System Design (ADS) were used for co-simulation. In simulation, we used the equivalent circuit model of varactor SMV-1233 provided manufacturer [24]. The manufactured prototypes were measured to verify performance using Keysight N5224 PNA vector network analyzer.

A. FILTER A: 50-TO-50 Ω TUNABLE BPF

Filter A is designed with input and output port impedances of 50 Ω. Other specifications of filter A, including the location of TZ in lower stopband are provided in section II. The circuit parameters of filter A are provided in Table 1. The physical layout and a photograph of the fabricated filter are presented in Fig. 18. Since the value of C_c is small, the cross-coupling between resonator R_1 and R_3 is implemented by controlling the gap (g_{sL}) in the fabricated filter.

Fig. 19 shows the simulation and measurement results of filter A. The measurement results are summarized in Table 2. The measured results are consistent with the simulation results. In the experiment, the passband frequency of filter A can be tuned from 1.65 GHz to 2.08 GHz by varying the bias voltage of 15 V to 0 V. The measured insertion loss (IL) varied from 3.42 dB to 4.64 dB, and the input and output return losses (RLs) were higher than 11 dB in each tuning state. The 3-dB bandwidth varied from 95 MHz to 120 MHz as the passband frequency is tuned from 1.65 GHz to 2.08 GHz. The TZ was located at a lower stopband frequency, indicated good selectivity of filter.

The power handling and nonlinearity of the proposed tunable BPF are mainly limited by nonlinearity of varactor diodes. To characterize nonlinearity, the input third-order intercept point (IIP3) is measured by using two-tone signal separated by 1 MHz. At each tuning state, the measured IIP3 is greater than 18 dBm.

B. FILTER B: 20-TO-50 Ω TUNABLE BPF

Filter B was designed with input port impedance $Z_S = 20$ Ω and output port impedance $Z_L = 50$ Ω. Other specifications relevant to filter B, including the location of TZ in lower stopband, are provided in section II. Fig. 20 presents the physical layout and a photograph of the fabricated filter B. The measurement of tunable BPF with arbitrary termination impedances (Z_s and $Z_L \neq 50$ Ω) were performed as follows:

a) Calibrate network analyzer for desired frequency range. After calibration, the effect of 50 Ω SMA connectors is eliminated by performing the port extension in network analyzer. The port extension function of network analyzer allows to move the measurement reference plane.
b) Change port impedance of network analyzer to desired value (*e.g.* port 1 = 25 Ω or 25+j10, port 2 = 50 Ω) and enable Z-port conversion function using fixture feature of network analyzer.
c) Finally, perform measurements and extract results. Using this procedure, we can verify performance of microwave circuits with any arbitrary termination impedances.

The simulation and measurement results of filter B are shown in Fig. 21, with summary of the measurement results provided in Table 2. The passband frequency is tuned from

TABLE 2. Measurement results of proposed tunable BPF with arbitrary termination impedances.

			Filter A: 50-to-50 Ω				Filter B: 20-to-50 Ω				Filter C: (25+j10)-to-50 Ω			
V_{dc} (V)	Tuning state	f_0 (GHz)	IL (dB)	RL (dB)	BW (MHz)	TZ (GHz)	IL (dB)	RL (dB)	BW (MHz)	TZ (GHz)	IL (dB)	RL (dB)	BW (MHz)	TZ (GHz)
15	T1	2.06	3.42	11.2	120	1.765	3.06	11.10	116	1.720	2.78	18.78	116	1.668
6.36	T2	1.95	3.44	14.36	115	1.640	3.43	16.49	110	1.652	3.27	21.07	108	1.580
4.15	T3	1.85	3.51	16.26	110	1.560	3.48	18.64	104	1.544	3.54	28.79	112	1.492
2.36	T4	1.75	3.81	24.48	105	1.470	3.81	20.92	100	1.476	3.80	25.05	100	1.420
0	T5	1.65	4.64	20.25	95	1.390	4.69	21.52	92	1.396	4.67	20.54	96	1.340

BW : 3-dB bandwidth, RL: Return loss at f_0, TZ: Transmission zero location frequency.

TABLE 3. Performance comparison between the design proposed in this work and previously reported works.

	FTR (GHz)	Z_S/Z_L (Ω)	IL (dB)	3-dB BW (MHz)	No of varactors	No. of dc-bias	Circuit size
[9]	1.10 ~ 2.10	50-to-50	4.4 ~ 6.10	40 ~ 44	9	5	$0.320\lambda_g \times 0.160\lambda_g$
[11]	1.7 ~ 2.70	50-to-50	3.8 ~ 4.9	50 ~ 110**	7	4	$0.120\lambda_g \times 0.070\lambda_g$
[12]	0.97 ~ 1.53	50-to-50	2 ~ 4.2	54 ~ 84**	6	1	$0.090\lambda_g \times 0.10\lambda_g$
[14]	1.25 ~ 2.10	50-to-50	3.5 ~ 6.50	54 ~ 162	16	5	NA
[16]	0.8 ~ 1.21	50-to-50	2 ~ 2.3	~ 130	10	4	$0.143\lambda_g \times 0.122\lambda_g$
[17]	0.88 ~1.13	50-to-50	3.2 ~4.3	46.8±3.4	4	1	NA
[18]	1.52 ~ 2.91	50-to-50	1.7 ~ 3.20	NA	3	1	$0.110\lambda_g \times 0.080\lambda_g$
[20]	1.21 ~ 1.585	50-to-50	2.8 ~ 3.70	133±1	4	2	$0.508\lambda_g \times 0.183\lambda_g$
This work^{I}	**1.65 ~ 2.08**	**50-to-50**	**3.42 ~ 4.64**	**95 ~ 120**	**3**	**1**	$0.261\lambda_g \times 0.260\lambda_g$
This work^{II}	**1.65 ~ 2.05**	**20-to-50**	**3.06 ~ 4.69**	**96 ~ 116**	**3**	**1**	$0.254\lambda_g \times 0.260\lambda_g$
This work^{III}	**1.65 ~ 2.05**	**(25+j10)-to-50**	**2.78 ~ 4.67**	**96 ~ 116**	**3**	**1**	$0.248\lambda_g \times 0.260\lambda_g$

FTR : Passband frequency tunability range, IL = maximum insertion loss within passband.

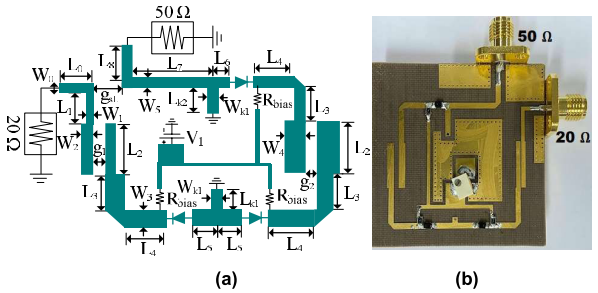

FIGURE 20. (a) Physical layout and (b) photograph of fabricated filter B. Physical dimenstions: $W_0 = W_1 = 0.85$, $W_2 = 0.72$, $W_3 = 1.36$, $W_{k1} = 1.3$, $W_4 = 1.71$, $W_5 = 1.36$, $L_0 = 6$, $L_1 = 8$, $L_2 = 10.76$, $L_3 = 8$, $L_4 = 8$, $L_5 = 5.97$, $L_{k1} = 1.3$, $L_{k2} = 6.40$, $L_6 = 1.05$, $L_7 = 11.35$, $L_8 = 9$, $g_1 = 0.13$, $g_2 = 1.08$, $g_{sL} = 3.13$. Unit: millimeter (mm).

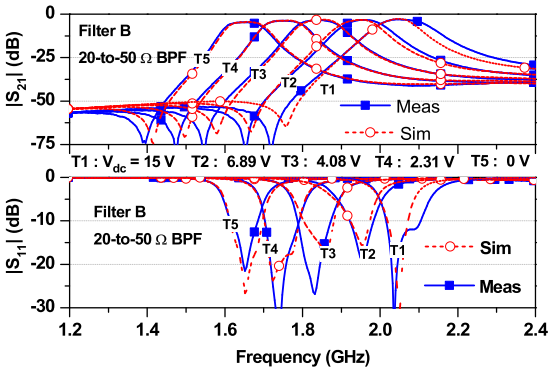

FIGURE 21. Simulation and measurement results of filter B: 20-to-50 Ω.

1.65 GHz to 2.06 GHz by varying the bias voltage of 0 V to 15 V. The measured IL varied from 3.06 dB to 4.69 dB. The input and output RLs were higher than 11 dB in each tuning state. The 3-dB bandwidth varied from 92 MHz to 116 MHz while tuning passband frequency of BPF.

C. FILTER C: (25+j10)-TO-50 Ω TUNABLE BPF

The design of filter C includes an input port impedance $Z_S = 25+j10$ Ω and output port impedance $Z_L = 50$ Ω. The filter specification is provided in section II. Additionally, the physical layout and a photograph of the fabricated can be seen in Fig. 22.

The simulation and measurement results of filter C are shown in Fig. 23. The measured results summarized in Table 2 and are consistent with the simulation results. The passband frequency tuned from 1.65 GHz to 2.06 GHz, with the measured IL varying from 2.78 dB to 4.67 dB. The input and output RLs were higher than 18 dB in each tuning state. The 3-dB bandwidth varied from 96 MHz to 116 MHz when the passband frequency is tuned from 1.65 GHz to 2.06 GHz. The TZ is located at a lower stopband which provides better selectivity.

Table 3 presents performance comparison of the proposed frequency tunable BPF with state-of-the arts alternatives. Previous reported works demonstrated the tunable BPFs, but

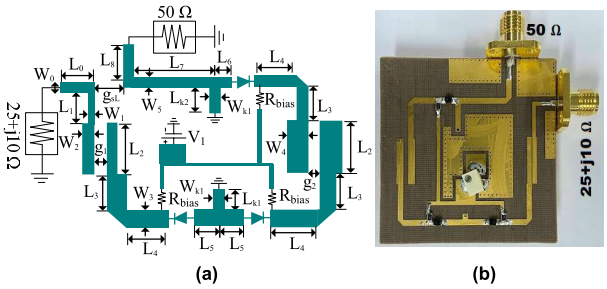

FIGURE 22. (a) Physical layout and (b) photograph of fabricated filter C. Physical dimenstions: $W_0 = W_1 = 1$, $W_2 = 0.80$, $W_3 = 1.36$, $W_{k1} = 1.3$, $W_4 = 1.71$, $W_5 = 1.36$, $L_0 = 6$, $L_1 = 5$, $L_2 = 10.50$, $L_3 = L_4 = 8$, $L_5 = 5.97$, $L_{k1} = 1.3$, $L_{k2} = 6.40$, $L_6 = 1.05$, $L_7 = 11.35$, $L_8 = 9$, $g_1 = 0.13$, $g_2 = 1.08$, $g_{sL} = 3.13$. Unit: milimeter (mm).

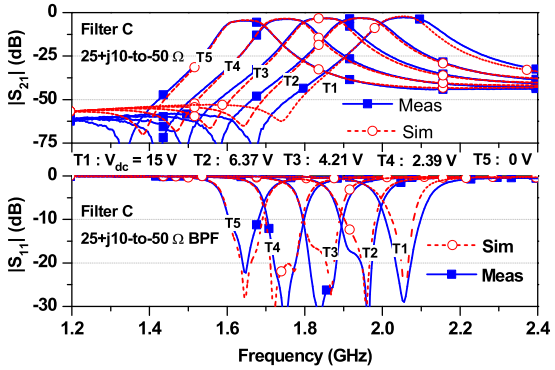

FIGURE 23. Simulation and measurement results of filter C: (25+j10)-to-50 Ω.

they mainly focused on input and output port impedances ($Z_S = Z_L = 50\ \Omega$) of 50 Ω. Furthermore, these designs required more than two dc-bias controlled signals, with the exception of the designs in [17], which had a complex structure for controlling resonators and/or individual inter-resonator coupling. In contrast, the proposed work demonstrated a frequency tunable BPF with TZ and arbitrary input and output port impedances ($Z_S \neq Z_L$), capable of integrating tunable BPF and matching network functions into a single circuit and allowing circuit size reduction of RF front-end. The TZ can be located near the passband either at lower or upper stopband to improve selectivity. Additionally, the passband frequency of the proposed BPF can be tuned with single dc-bias, simplifying the structure design, allowing lower fabrication cost, and making it less sensitive to fabrication tolerance.

V. CONCLUSION

In this work, we presented a novel design of tunable BPF that allows for arbitrary terminated input and output ports impedances and includes transmission zero. We have developed a filter design theory based on an existing cross-coupling CM filter theory and performed an intuitive circuit-level implementation using quarter-wave microstrip line tunable resonators controlled by single dc-bias. The proposed tunable BPF integrates the function of frequency selective characteristics of tunable BPF and matching networks into single circuit, resulting overall circuit size reduction of RF front-end. The effect of frequency-dependent input/output port impedances was also demonstrated. To experimentally validate the design, three microstrip line filters (filter A: 50-to-50 Ω, filter B: 20-to-50 Ω, and filter C: (25+j10)-to-50 Ω) were designed and fabricated. The simulation and experimental results showed good agreement.

REFERENCES

[1] K. Chen, J. Lee, W. J. Chappell, and D. Peroulis, "Co-design of highly efficient power amplifier and high-*Q* output bandpass filter," *IEEE Trans. Microw. Theory Techn.*, vol. 61, no. 11, pp. 3940–3950, Nov. 2013.

[2] K. Chen, T. C. Lee, and D. Peroulis, "Co-design of multi-band high efficiency power amplifier and three-pole high-*Q* tunable filter," *IEEE Microw. Wireless Compon. Lett.*, vol. 23, no. 12, pp. 647–649, Dec. 2013.

[3] Y. Gao, X. Shang, C. Guo, J. Powell, Y. Wang, and M. J. Lancaster, "Integrated waveguide filter amplifier using the coupling matrix technique," *IEEE Microw. Wireless Compon. Lett.*, vol. 29, no. 4, pp. 267–269, Apr. 2019.

[4] P. Pech, P. Kim, and Y. Jeong, "Microwave amplifier with substrate integrated waveguide bandpass filter matching network," *IEEE Microw. Wireless Compon. Lett.*, vol. 31, no. 4, pp. 401–404, Apr. 2021.

[5] J. A. Estrada, J. R. Montejo-Garai, P. de Paco, D. Psychogiou, and Z. Popovic, "Power amplifiers with frequency-selective matching networks," *IEEE Trans. Microw. Theory Techn.*, vol. 69, no. 1, pp. 697–708, Jan. 2021.

[6] H. Meng, P. Zhao, K. Wu, and G. Macchiarella, "Direct synthesis of complex loaded Chebyshev filters in a complex filtering network," *IEEE Trans. Microw. Theory Techn.*, vol. 64, no. 12, pp. 4455–4462, Dec. 2016.

[7] M. Meng and K. L. Wu, "Direct synthesis of general Chebyshev bandpass filters with a frequency variant complex load," in *IEEE MTT-S Int. Microw. Symp. Dig.*, May 2010, pp. 433–436.

[8] P. Kim and Y. Jeong, "A new synthesis and design approach of a complex termination impedance bandpass filter," *IEEE Trans. Microw. Theory Techn.*, vol. 67, no. 6, pp. 2346–2354, Jun. 2019.

[9] C. Chen, G. Wang, and J. Li, "Microstrip switchable and fully tunable bandpass filter with continuous frequency tuning range," *IEEE Microw. Wireless Compon. Lett.*, vol. 28, no. 6, pp. 500–502, Jun. 2018.

[10] F. Lin and M. Rais-Zadeh, "Continuously tunable 0.55–1.9-GHz bandpass filter with a constant bandwidth using switchable varactor-tuned resonators," *IEEE Trans. Microw. Theory Techn.*, vol. 65, no. 3, pp. 792–803, Mar. 2017.

[11] P. Chi, T. Yang, and T. Tsai, "A fully tunable two-pole bandpass filter," *IEEE Microw. Wireless Compon. Lett.*, vol. 25, no. 5, pp. 292–294, May 2015.

[12] L. Gao and G. M. Rebeiz, "A 0.97–1.53-GHz tunable four-pole bandpass filter with four transmission zeroes," *IEEE Microw. Wireless Compon. Lett.*, vol. 29, no. 3, pp. 195–197, Mar. 2019.

[13] Y. Cho and G. M. Rebeiz, "Tunable 4-pole noncontiguous 0.7–2.1-GHz bandpass filters based on dual zero-value couplings," *IEEE Trans. Microw. Theory Techn.*, vol. 63, no. 5, pp. 1579–1586, May 2015.

[14] T. Yang and G. M. Rebeiz, "Tunable 1.25–2.1-GHz 4-pole bandpass filter with intrinsic transmission zero tuning," *IEEE Trans. Microw. Theory Techn.*, vol. 63, no. 5, pp. 1569–1578, May 2015.

[15] G. Zhang, Y. Xu, and X. Wang, "Compact tunable bandpass filter with wide tuning range of center frequency and bandwidth using short-coupled lines," *IEEE Access*, vol. 6, pp. 2962–2969, 2018.

[16] D. Lu, X. Tang, N. S. Barker, M. Li, and T. Yan, "Synthesis-applied highly selective tunable dual-mode BPF with element-variable coupling matrix," *IEEE Trans. Microw. Theory Techn.*, vol. 66, no. 4, pp. 1804–1816, Apr. 2018.

[17] M. Ohira, S. Hashimoto, Z. Ma, and X. Wang, "Coupling-matrix-based systematic design of single-DC-bias-controlled microstrip higher order tunable bandpass filters with constant absolute bandwidth and transmission zeros," *IEEE Trans. Microw. Theory Techn.*, vol. 67, no. 1, pp. 118–128, Jan. 2019.

[18] T. Lim, A. Anand, J. Chen, X. Liu, and Y. Lee, "Design method for tunable planar bandpass filters with single-bias control and wide tunable frequency range," *IEEE Trans. Circuits Syst. II, Exp. Briefs*, vol. 68, no. 1, pp. 221–225, Jan. 2021.
[19] R. Allanic, D. Le Berre, Y. Quere, C. Quendo, D. Chouteau, V. Grimal, D. Valente, and J. Billoue, "A novel synthesis for bandwidth switchable bandpass filters using semi-conductor distributed doped areas," *IEEE Access*, vol. 8, pp. 122599–122609, 2020.
[20] D. Lu, M. Yu, N. S. Barker, Z. Li, W. Li, and X. Tang, "Advanced synthesis of wide-tuning-range frequency-adaptive bandpass filter with constant absolute bandwidth," *IEEE Trans. Microw. Theory Techn.*, vol. 67, no. 11, pp. 4362–4375, Nov. 2019.
[21] R. J. Cameron, C. M. Kudsia, and R. R. Mansour, *Microwave Filters for Communication Systems: Fundamentals, Design and Applications*. Hoboken, NJ, USA: Wiley, 2007.
[22] J. S. Hong, *Microstrip Filters for RF/Microwave Applications*. Hoboken, NJ, USA: Wiley, 2011.
[23] G. Chaudhary and Y. Jeong, "Frequency tunable impedance matching non-reciprocal bandpass filter using time-modulated quarter-wave resonators," *IEEE Trans. Ind. Electron.*, vol. 69, no. 8, pp. 8356–8365, Aug. 2022.
[24] *SMV123x Series: Hyper-Abrupt Junction Tuning Varactors*, Skyworks Inc., Irvine, CA, USA, 2012.

GIRDHARI CHAUDHARY (Member, IEEE) received the B.E. degree in electronics and communication engineering from the Nepal Engineering College (NEC), Kathmandu, Nepal, in 2004, the M.Tech. degree in electronics and communication engineering from the MNIT, Jaipur, India, in 2007, and the Ph.D. degree in electronics engineering from Jeonbuk National University, Republic of Korea, in 2013.

He is currently a Contract Professor with the JIANT-IT Human Resource Development Center, Jeonbuk National University. Previously, he was a Principal Investigator on an independent project through the Basic Science Research Program administrated by the National Research Foundation (NRF) and funded by the Ministry of Education. His research interests include multi-band tunable passive circuits, in-band full duplex systems, high efficiency power amplifiers, and applications of negative group delay circuits. He was a recipient of the BK21 PLUS Research Excellence Award from the Korean Ministry of Education, in 2015. He was a recipient of the Korean Research Fellowship (KRF) through the NRF funded by the Ministry of Science and ICT.

YONGCHAE JEONG (Senior Member, IEEE) received the B.S.E.E., M.S.E.E., and Ph.D. degrees in electronics engineering from Sogang University, Seoul, Republic of Korea, in 1989, 1991, and 1996, respectively.

From 1991 to 1998, he was a Senior Engineer with Samsung Electronics, Seoul. Since 1998, he has been with the Division of Electronics Engineering, Jeonbuk National University, Jeonju, Republic of Korea. From July 2006 to December 2007, he was a Visiting Professor with the Georgia Institute of Technology. He was the Director of the HOPE-IT Human Resource Development Center, BK21 PLUS, and the National University's Vice-President of Planning. He is currently a Professor with Jeonbuk National University. He has authored or coauthored over 260 papers in international journals and conference proceedings. His research interests include active and passive microwave circuits for mobile and satellite base-station RF systems, periodic defected transmission lines, negative group delay circuits and their applications, in-band full duplex radio, and RFIC design. He is a member of the Korea Institute of Electromagnetic Engineering and Science (KIEES).